Photothermal activation in the near infrared range for 4-dimensional printing using relevant organic dyes

Valentin Launay, Romain Wolff, Frédéric Dumur, Jacques Lalevée

Photothermal activation in the near infrared range for 4-dimensional printing using relevant organic dyes

Valentin Launay[1,2], Romain Wolff[1,2], Frédéric Dumur[3], Jacques Lalevée*[1,2]

[1]Université de Haute-Alsace, CNRS, IS2M UMR 7361, F-68100 Mulhouse, France
[2]Université de Strasbourg, France
[3]Aix Marseille Univ, CNRS, ICR UMR 7273, F-13397 Marseille, France
e-mail: jacques.lalevee@uha.fr

Abstract:

4D printing has become an exciting sector of 3D printing since its appearance in the 2010s. This technology consists in adding time as an extra dimension of 3D printing. Different stimuli can be used to modify a 3D object after the printing process such as solvent, temperature, magnetic field, electricity or light. In this paper, a 4D behaviour was investigated using NIR light in combination with a low amount of NIR organic dyes in-situ embedded in the 3D printed polymer. As a first step, the influence of several parameters on the photothermal effect generated have been followed such as the NIR dye structure, the NIR dye concentration, the irradiation wavelength, the light irradiance and the polymer matrix. Due to the light-triggered process, the deformation of the 3D printed object could be reversibly achieved in the presence of a NIR organic dye in a few amount of time (20 s). In fact, the photothermal effect in-situ generated in the 3D printed object allowed to reach a temperature above the T_g of the latter. This phenomenon has been highlighted with tensile tests. Indeed, these tests showed the passage of the 3D printed object from a glassy state to a rubbery state upon NIR irradiation. Finally, the photothermal effect produced was used to rapidly bond two parts of a broken 3D printed object.

1. Introduction

The popularity of 3D printing is steadily growing since its emergence in the 1980s thanks to the appeal of the layer-by-layer manufacturing technique. This technology is widely used for rapid prototyping in a wide range of fields from products of general consumption to more advanced applications such as medicine, electronics, fashion, construction or aerospace.[1-8] One of the main 3D printing techniques consists in using light in combination with a photosensitive resin to perform a layer-by-layer photopolymerization. For this purpose, SLA (stereolithography apparatus), DLP (digital light processing) and LCD (liquid crystal display) 3D printers are the most commonly used.[9-11]

However, 3D printing has limitations in spite of the considerable boom from the 1980s. First of all, printing chambers are quite small, limiting the printing of massive 3D objects that need to be printed in multiple runs, increasing the cost of production. Furthermore, the choice of materials to use is limited and depends on the type of 3D printers used. Thus, the printing of 3D objects is difficult in some fields such as food where the usable materials are restricted. In addition, the printed materials are often breakable, reducing the lifetime. Moreover, the recycling issues for 3D printed objects remains a major challenge. Finally, a post-curing step is often needed to improve the monomer conversion at the end of the polymerization. In fact, improvement of the monomer conversion increases the glass transition temperature (T_g) and the mechanical properties of the polymer.[12] Thus, the 3D printed sample is often placed in a UV chamber, a heat chamber or a microwave oven to complete the polymerization of the last unreacted monomers.[13][14] The final mechanical properties achieved depend on the equipment used, the type of post-processing and the duration of this latter.[15-17]

4D printing which is based on additive manufacturing appeared in this context. Indeed, Tibbits showed in 2013 a way to modify a static 3D object over time during a TED talk.[18] Since then, 4D printing has become an exciting sector of 3D printing, attracting more and more attention from scientists. 4D technology consists in adding an extra dimension to 3D printing: time. For this purpose, a material has to be developed in such a way that properties such as colour or shape of the 3D object after the printing process can be modified under a controllable external stimulus. Different stimuli can be used to this end such as solvent, pH,

temperature, magnetic field, electricity or light.[19-24] The aim is to be able to adapt the 3D object over time to change the functionality on demand.

In previous studies, we demonstrated the near-infrared (NIR) light being able to produce high photothermal effects in the presence of NIR organic dyes fully soluble in the polymer contrary to inorganic photothermal agents such as nanoparticles or graphene oxide.[25-27] These NIR organic dyes could be in-situ embedded into the polymer to enable a substantial increase of the polymer temperature above its T_g upon NIR irradiation. In the present work, we first studied the behaviour of six different NIR organic dyes covering a wide range of NIR absorption and three representative families (cyanine, squaraine and diammonium). Notably, we studied the optical properties of our NIR organic dyes and deepened the influence of different parameters on the photothermal effect generated. One of these NIR organic dyes was then selected in combination with a NIR light as stimulus to reach a 4D behaviour. Indeed, influence of the NIR dye on the mechanical properties of the 3D printed objects has been analyzed through tensile tests. Furthermore, the photothermal effect produced by the NIR dye in-situ embedded into the polymer was used to shape the 3D printed object. This shaping was reversible by reirradiation of the polymer upon the same NIR source.

2. Experimental section

2.1. Chemical compounds

Trimethylolpropane triacrylate (**TMPTA**) was purchased from Sigma-Aldrich, phenyl *bis*(2,4,6-trimethylbenzoyl)-phosphine oxide (**BAPO**) and ethyl (2,4,6-trimethylbenzoyl) phenylphosphinate (**TPO-L**) were obtained from Lambson Ltd (UK), 2-[2-[2-Chloro-3-[2-(1,3-dihydro-1,1,3-trimethyl-2*H*-benz[*e*]indol-2-ylidene)ethylidene]-1-cyclohexen-1-yl]ethenyl]-1,1,3-trimethyl-1*H*-benz[*e*]indolium 4-methylbenzenesulfonate (**IR-813**) was ordered from Tokyo Chemical Industry (TCI-Europe), methyl methacrylate (**MMA**) and crayvallac SLT were provided by Arkema, glycerol formal methacrylate (**GLYFOMA**) was supplied from Evonik, isobornyl methacrylate (**IBOMA**), 3,3,5-trimethyl cyclohexyl methacrylate (**TMCHMA**) and trimethylolpropane formal acrylate (**TMPFA**) were furnished by Startomer-Europe, isobornyl acrylate (**IBOA**) comes from Allnex, *H*-Indolium, 2-(2-(3-(2-(1,3-dihydro-1,3,3-trimethyl-2*H*-indol-2-ylidene)ethylidene)-2-((1-phenyl-1*H*-tetrazol-5-

yl)thio)-1-cyclohexen-1-yl)ethenyl)-1,3,3-trimethyl chloride (**IR-785**), 1-butyl-2-((1*E*,3*E*,5*Z*)-5-(1-butylbenzo[*cd*]indol-2(1*H*)-ylidene)penta-1,3-dien-1-yl)benzo[*cd*]indol-1-ium tetrafluoroborate (**IR-850**), 6-butoxy-2-((1*E*,3*E*,5*Z*)-5-(6-butoxy-1-butylbenzo[*cd*]indol-2(1*H*)-ylidene)penta-1,3-dien-1-yl)-1-butylbenzo[*cd*]indol-1-ium tetrafluoroborate (**IR-940**) and N^1,N^1,N^4,N^4–tetrakis(4-(dibutylamino)phenyl)benzene-1,4-diaminium hexafluoro-antimonate (**IR-1064**) were ordered from Lotte Chemical Pakistan Ltd (LOTCHEM). 2-[[2-Hydroxy-3-[(1-octylbenz[*cd*]indol-2(1*H*)-ylidene)methyl]-4-oxo-2-cyclobuten-1-ylidene]methyl]-1-octyl-benz[*cd*]indolium (**SQ**) was synthesized according to a procedure recently reported in the literature.[28] Chemical structures of the different monomers, photoinitiators and NIR organic dyes are presented in the Scheme 1 except that of the crayvallac SLT which was used as a thickener.

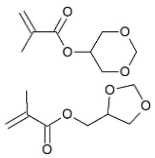

GLYFOMA

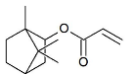

IBOA

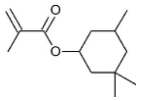

TMCHMA

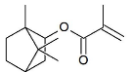

IBOMA

MMA

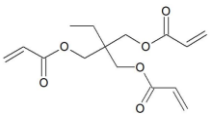

TMPTA

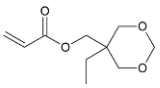

TMPFA

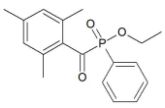

TPO-L

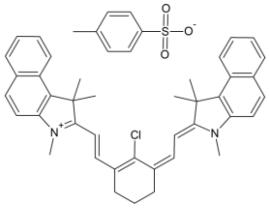

IR-813

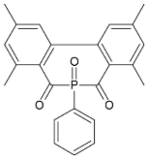

BAPO

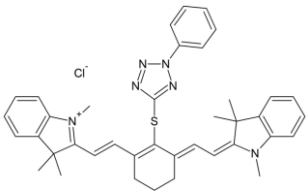

IR-785

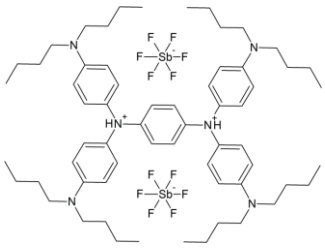

IR-1064

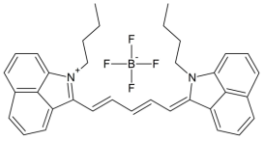

IR-850

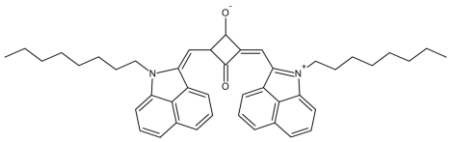

SQ

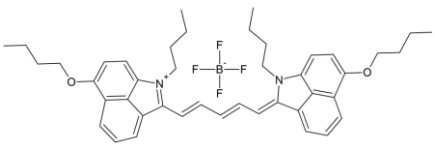

IR-940

Scheme 1. Chemical structures of monomers (GLYFOMA, IBOA, TMCHMA, IBOMA, MMA, TMPTA and SR531), photoinitiators (TPO-L and BAPO) and NIR organic dyes (IR-785, IR-813, IR-850, IR-940, IR-1064 and SQ) used in this study.

2.2. Polymerization in bulk followed by RT-FTIR spectroscopy

Polymer samples were prepared to test the heater effect for in-situ embedded NIR organic dyes. In order to prepare these samples, six different monomers (GLYFOMA, IBOA, TMCHMA, IBOMA, MMA and TMPTA) were mixed with a UV photoinitiator (BAPO for GLYFOMA, IBOA, TMCHMA, TMPTA and TPO-L for MMA). In addition, a heater - which is a NIR organic dye (IR-785, IR-813, IR-850, IR-940, IR-1064 or SQ, fully soluble in monomers) - was incorporated into the photocurable resin before being polymerized with a laser diode at 405 nm. For GLYFOMA, a thickener (crayvallac SLT) was added to control the viscosity of the photocurable sample.

Photopolymerization experiments enabling to access to polymers were carried out at room temperature upon irradiation with a laser diode at 405 nm (110 $mW.cm^{-2}$) in a mold covered by a polypropylene film to deny the oxygen inhibition. A Jasco 6600 real-time Fourier transformed infrared spectroscopy (RT-FTIR) was used to monitor the C=C acrylate double bond conversion between 6100 and 6200 cm^{-1} during the irradiation time. Polymer films with a thickness of 2 mm were prepared in these experiments.

2.3. UV-VIS absorption spectroscopy

A Jasco V-730 spectrophotometer was used to measure the visible-NIR absorption spectra of NIR dyes in acetonitrile, toluene, GLYFOMA and polyGLYFOMA.

2.4. Heater effect followed by infrared thermal imaging camera

In order to follow the heater effect of the NIR dyes in-situ embedded into polymer samples, different NIR light sources were used. Indeed, laser diodes were used at 785 nm, 940 nm, 980 nm and 1064 nm and a LED was used at 850 nm. A Phoseon NIR LED panel was also used at 810 nm for larger irradiations. Excitations with the NIR light source were done at a distance of 2 cm for the laser diodes and 6 cm for the LED. A Fluke TiX500 infrared thermal imaging camera was used to follow in real time the temperature reached by the polymer.

2.5. Thermogravimetric analysis (TGA)

The Mettler Toledo TGA DSC 3+ and the Star software were used to measure the thermal decomposition temperature of NIR organic dyes under air. These latter were heated from 30°C to 900°C with a rise in temperature of 10 $K.min^{-1}$.

2.6. Polymer preparation with a 3D LCD printer

In order to get 3D polymers, a blend between $\frac{3}{4}$ of SR531 and $\frac{1}{4}$ of IBOA was realised in order to increase the T_g of the final polymer (T_g of SR531 is around 10°C). Then, $2\%_{wt}$ of photoinitiator (BAPO) and $0.1\%_{wt}$ of NIR dye (IR-813) were added to the photosensitive system before the printing process. The photopolymerization step was performed with a 3D LCD printer, ANYCUBIC Photon S. 3D modelizations were created with the software ANYCUBIC Photon Slicer. Thanks to a LED and a 2K LCD screen, this printer is able to carry photopolymerizations at 405 nm with a low irradiance (some $mW.cm^{-2}$). The XY resolution of the printer is 0.047 mm with a Z precision of 0.00125 mm. The 3D model used is given in Figure S1, Supporting Information. Thickness of the final 3D objects is 2 mm. Finally, a post-curing step was performed on 3D printed objects consisting in irradiating samples for 1 h at 395 nm (130 $mW.cm^{-2}$).

2.7. Tensile tests

The ZwickRoell dynamometer and the testXpert III software were used to perform tensile tests of the 3D printed objects. The speed spacing was fixed at 10 $mm.min^{-1}$ with an initial spacing between jaws of 40 mm. The experimental set-up is presented in Figure S2, Supporting Information. Some samples were irradiated 3 min before the experiment with a NIR LED panel at 810 nm. The sample was still irradiated during the tensilte test to know the mechanical properties of the 3D objects upon NIR light.

3. Results and discussion

3.1. Characterization of the photothermal effect

The first part of this work focuses on a deepen study of the photothermal effect generated in-situ in polymers. For this purpose, influence of several parameters such as the NIR dye structure, the NIR dye concentration, the wavelength of the NIR irradiation, irradiance of the NIR source and polymers in which NIR dyes are embedded have been

studied on the photothermal effect generated. The strategy used to produce an important photothermal effect is described in the Scheme 2. First, the NIR organic dye was mixed up with the photosensitive system. Then, the blend was photopolymerized with an ultraviolet (UV) source at 405 nm to be representative of the most common 3D printer sources. At this stage, the NIR organic dye is therefore useless but has to stay inert and should affect as few as possible the photopolymerization kinetics (inner filter effect, chemical reactions...). Once the photopolymerization performed, NIR dye molecules are embedded in the polymer network. Usefulness of the NIR dye comes when the polymer is irradiated upon NIR light. Indeed, they are able to convert light into heat within the polymer by thermal relaxation and thus reach applications and functionalities previously impossible to acquire such as polymer shaping (4D behaviour).

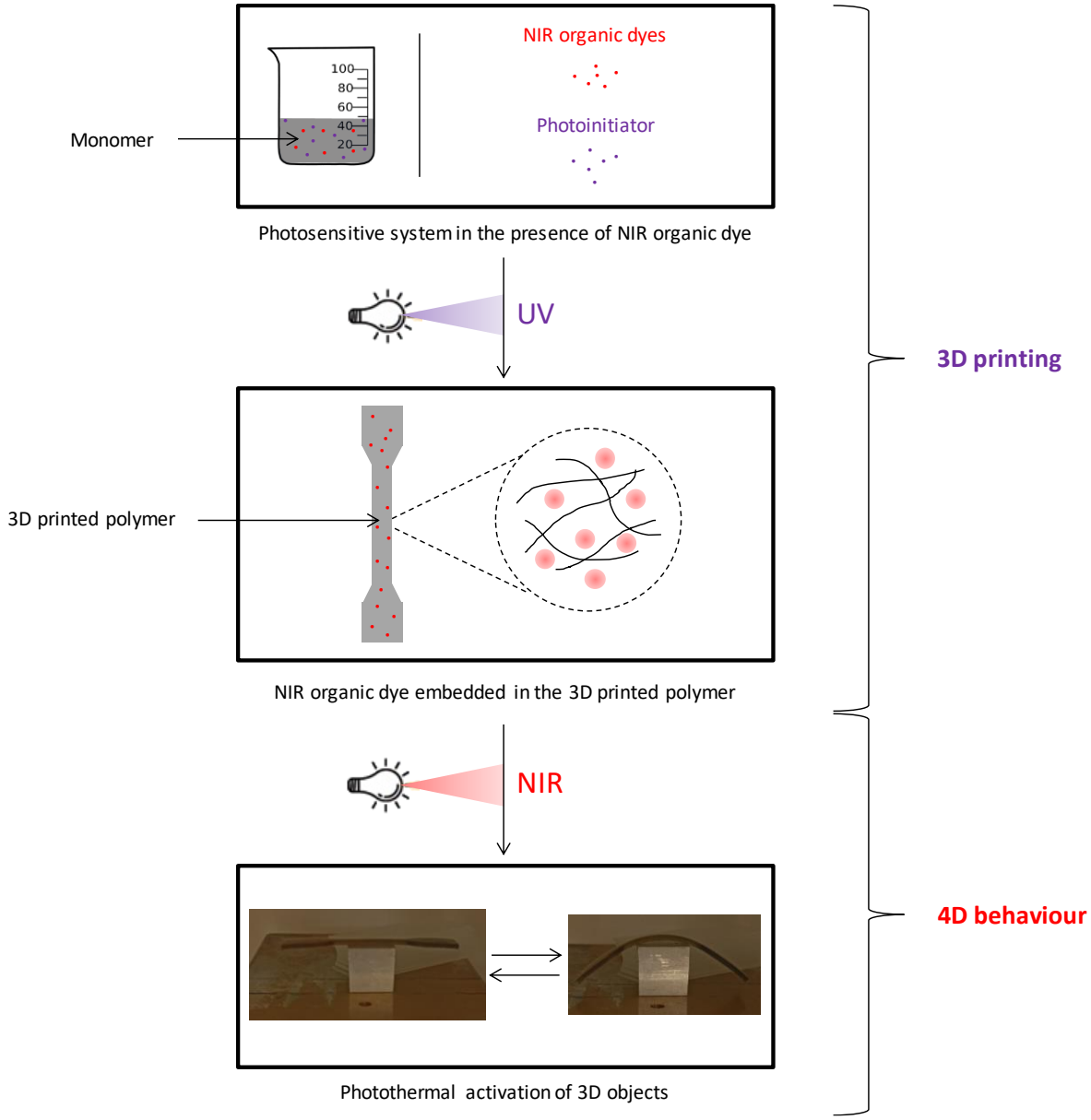

Scheme 2. Strategy used to produce a high photothermal effect.

Absorption spectra of NIR dyes have been determined in the Visible-NIR range by UV-Visible absorption spectroscopy in acetonitrile and toluene (Figure S3-8 and Table S1, Supporting Information). They are easily soluble in each solvent. First, it is interesting to note the position of the absorption peaks as well as the absorption ranges of the different NIR dyes. Thus, the latter covers a wide absorption range extending from 650 nm to more than 1100 nm. The solvent also has an influence on the optical properties of the dyes. Indeed, bathochromic and hypsochromic effects from some nm as for IR-785 to more than 100 nm as for IR-1064. Furthermore, some dyes have a much higher affinity in some solvents than in other ones.

The photothermal effect being generated after polymerization, it is important to know the absorption properties of our NIR dyes in the polymer. Thus, NIR absorption spectra have been performed in polyGLYFOMA and GLYFOMA and presented in Figure 1 and Figure S9, Supporting Information. Table S2 and Table S3 summarize maximal wavelengths of the different dyes and their molar extinction coefficients at 785 nm considering they were not degraded during the polymerization process. Overall, the absorption range of NIR dyes trends to widen when the photopolymerization is completed, allowing better absorption properties in polyGLYFOMA than GLYFOMA at wavelengths distant from the absorption peak. IR-813 molar extinction coefficient is the best of the six NIR dyes studied at 785 nm. Therefore, we expect the photothermal effect generated to be higher in the presence of IR-813 than for the other ones. Moreover, the temperature reached by the polymer in presence of IR-940 should be lower since its molar extinction coefficient is substantially lower in comparison with other NIR dyes. However, the photothermal effect generated depends on the photothermal conversion of NIR dyes which is the efficiency with which a photothermal agent can transfer light to heat to a system upon NIR light.[29]

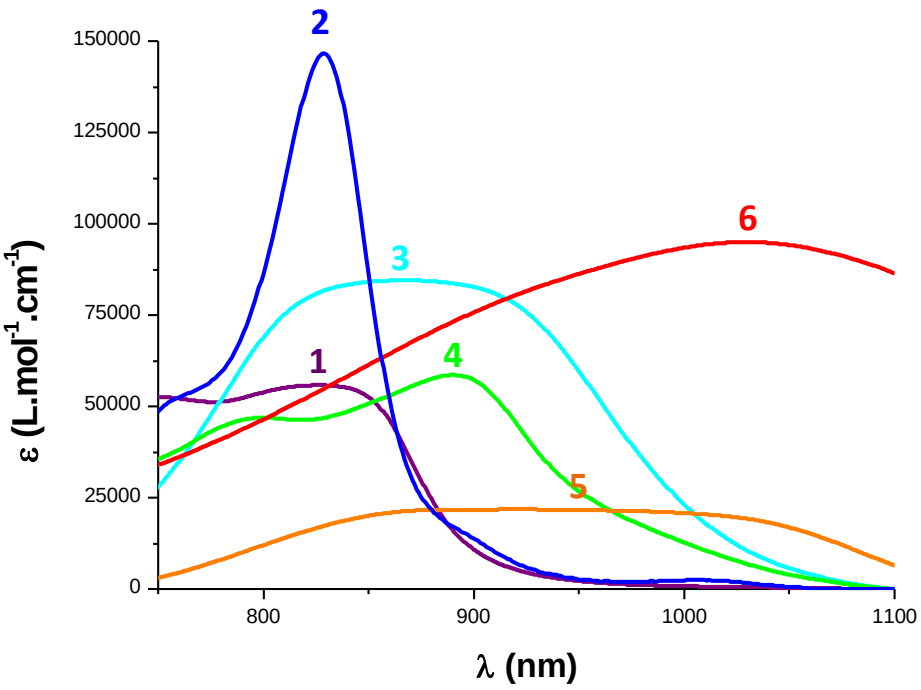

Figure 1. NIR spectra comparison of (1) IR-785, (2) IR-813, (3) IR-850, (4) SQ, (5) IR-940 and (6) IR-1064 in polyGLYFOMA.

After the obtention of the GLYFOMA-based polymers following the strategy depicted in Scheme 2, photothermal effect generated upon NIR light has been studied. In this aim, temperature profiles of reference polymers without NIR dye have been compared with polymers containing 0.1%$_{wt}$ of NIR dye upon NIR light at 785 nm (2 W.cm^{-2}). Temperature data are collected using a thermal imaging camera (Figure 2). As expected, the photothermal effect generated in the presence of NIR dye is much higher than in the reference polymer. Indeed, the temperature reached in the reference polymer does not exceed 35°C whereas the temperature in the presence of NIR dyes is always higher than 110°C. The NIR dye producing the best photothermal effect is IR-813 (188°C) according to a better molar extinction coefficient as shown in Table S4, Supporting Information. Apart from IR-813, IR-785 and IR-850 generate the most important photothermal effects (142°C and 132°C respectively). However, IR-785 produces a better photothermal effect despite a lower molar extinction coefficient. This result indicates a better photothermal conversion for IR-785 than IR-850 in this polymer. Finally, SQ generates the lowest photothermal effect in spite of a proper molar extinction coefficient. The photothermal conversion of SQ is therefore low. This phenomenon can be ascribed to the trend of squaraines to come back to their ground state by fluorescence, denying the light-to-heat conversion.[30]

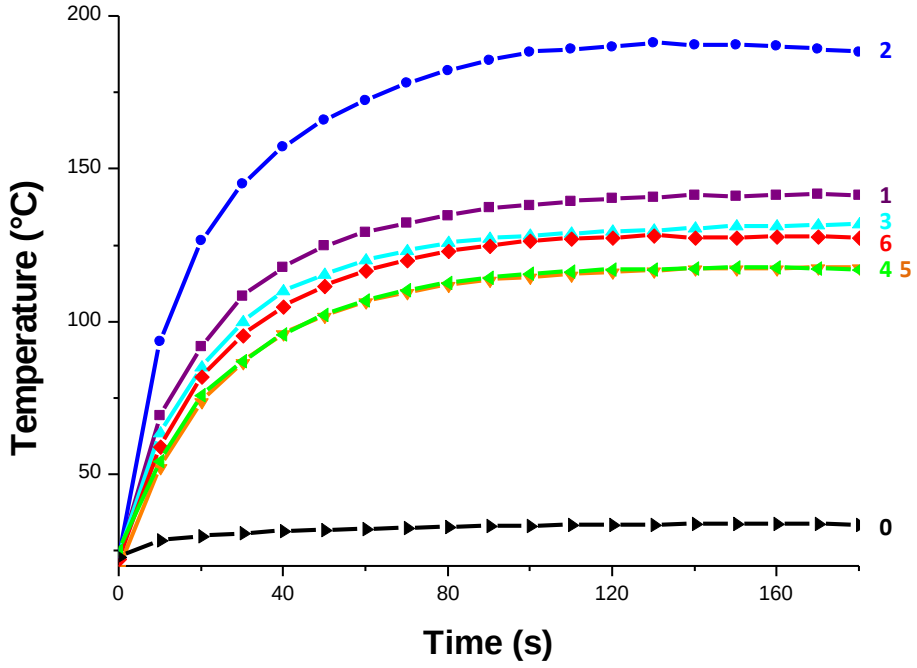

Figure 2. Photothermal effect generated upon NIR light at 785 nm (2 W.cm^{-2}) in polyGLYFOMA (0) Without NIR dye ; with 0.1%$_{wt}$ of (1) IR-785, (2) IR-813, (3) IR-850, (4) SQ, (5) IR-940 et (6) IR-1064.

Temperatures reached by the polymer in the presence of NIR dyes upon NIR light are high, this is the reason why it is crucial to know the thermal degradation of the latter. Thus, their thermal properties have been analyzed with TGA. NIR dyes were subjected to a temperature ramp ranging from 30°C to 700°C with a rising temperature of 10 $K.min^{-1}$ (Figure S10-15, Supporting Information). NIR dyes used being hygroscopic, it will be considered that there is no degradation of the polymer sample up to 10% loss of mass. Table 1 summarize degradation temperatures following this criterion. In the analysis conditions, NIR dyes keep a good shape until temperatures far above temperatures required to overcome the T_g of most usual polymers. Indeed, NIR dyes keep an excellent thermal stability until 238°C to 321°C. These high temperatures ensure good stability and therefore reactivability for many irradiation cycles in the material.

Table 1. Thermal degradation temperature of NIR dyes determined by TGA.

Colorant	$T_{10\%}$ (°C)
IR-850	238
IR-813	252
IR-785	272
IR-1064	290
IR-940	320
SQ	321

Then, influence of the concentration on the photothermal effect generated has been studied. First, photopolymerizations of TMPTA-based resins have been recorded by RT-FTIR to monitor the C=C double bond conversion of the acrylate function at several NIR dye concentrations. As shown in Figures S16-21, Supporting Information, conversions of the photosensitive resins are lowly affected by NIR dyes until a threshold concentration. Thus, photopolymerizations are weakly affected for concentrations under $0.2\%_{wt}$ for IR-785, IR-813 and IR-850, $0.1\%_{wt}$ for SQ, $0.08\%_{wt}$ for IR-940 and $0.05\%_{wt}$ for IR-1064. This phenomenon

can be ascribed to the absorption of photons at 405 nm by NIR dyes or by an inner filter effect.

Next, TMPTA-based polymers were prepared at several NIR dye concentrations and irradiated at 785 nm (2.55 $W.cm^{-2}$). As shown in Figure 3, the NIR dye concentration required to produce an important photothermal effect is low (around 0.05-0.1%$_{wt}$). Indeed, a linear correlation can be established for the whole NIR dyes between the temperature reached upon NIR light and the NIR dye concentration logarithm. The coefficients of determination r^2 of these NIR dyes fluctuate from 0.92 to 0.98. Beyond 0.1%$_{wt}$, the temperature gain is less important.

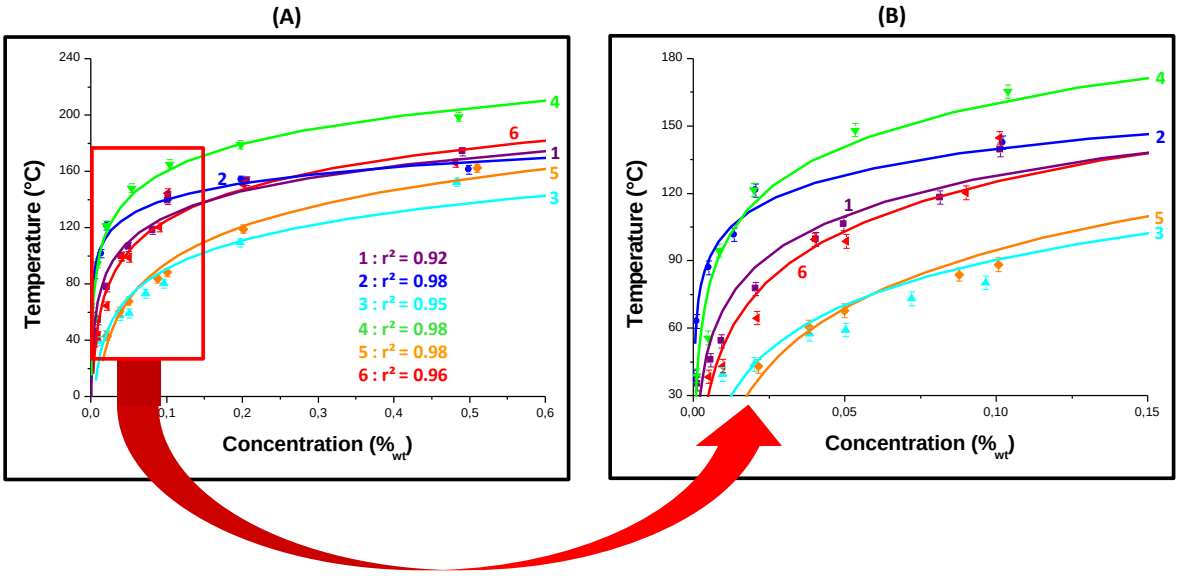

Figure 3. Maximal temperatures reached by polyTMPTA for different concentrations of (1) IR-785, (2) IR-813, (3) IR-850, (4) SQ, (5) IR-940 et (6) IR-1064 upon NIR irradiation at 785 nm (2.55 $W.cm^{-2}$) on a (A) linear and (B) logarithmic scale.

Thereafter, influence of the irradiation wavelength on the photothermal effect generated has been studied. To that end, NIR dyes were analyzed in polyGLYFOMA at different irradiation wavelengths (785 nm, 850 nm, 940 nm, 980 nm and 1064 nm). First, the polyGLYFOMA without and with 0.1%$_{wt}$ of NIR dye have been irradiated at 1 $W.cm^{-2}$ at the aforesaid wavelengths (Figure 4). Different behaviors can be observed, depending on the irradiation wavelength. Indeed, IR-785 and IR-813 dyes are very efficient for short NIR wavelengths but this efficiency worsen for high NIR wavelengths. On the opposite, IR-940 and IR-1064 dyes are not very efficient for short NIR wavelengths but this efficiency

improves for high NIR wavelengths. For SQ, no general trend seems to emerge regarding the efficiency at the different NIR wavelengths studied. Finally, the efficiency of IR-850 increases up to 850 nm and then stabilizes at higher wavelengths.

Beyond the behaviour of these dyes, some are inherently more efficient than others. Thus, temperatures reached by the polymer in the presence of IR-785, SQ and IR-1064 are surpassed by the other dyes at all the wavelengths studied. Indeed, IR-813 is the most interesting NIR dye between 785 nm and 850 nm whereas IR-850 is the most interesting one between 850 nm and 940 nm. Finally, the most interesting NIR dye between 940 nm and 1064 nm is IR-940.

Lastly, temperatures reached by polyGLYFOMA in the presence of each NIR dyes after 3 min of NIR irradiation at 1 W.cm^{-2} were linked to their molar extinction coefficients (Figure S22, Supporting Information). Thus, the molar extinction coefficient does not have to be very high to achieve a good photothermal effect. Thermal relaxation phenomena through the photothermal conversion will play a key role depending on the NIR dye structure. Furthermore, this figure shows that the higher the molar extinction coefficient is, the higher the generated temperature is guaranteed to be.

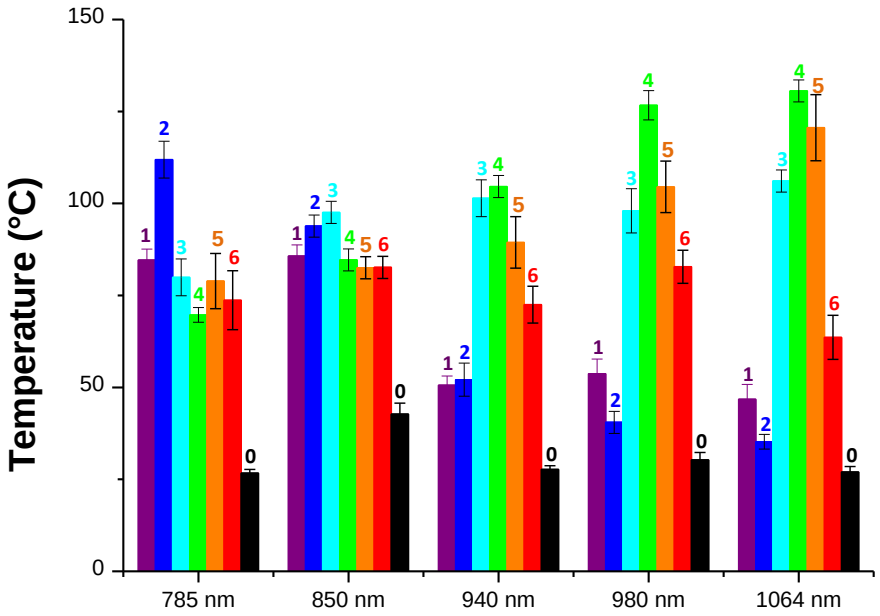

Figure 4. Temperature as a function of the light source wavelength (I = 1 W.cm^{-2}) for polyGLYFOMA : (0) without NIR dye ; with 0.1%$_{wt}$ of (1) IR-785, (2) IR-813, (3) IR-850, (4) SQ, (5) IR-940, (6) IR-1064. Temperatures are recorded after 3 min of NIR irradiation.

Then, influence of the NIR source irradiance on the photothermal effect has been investigated. First, polyGLYFOMA samples have been irradiated at several irradiances and wavelengths for the whole NIR dyes studied and the reference (polymer without NIR dye). Examples with temperature profiles of polyGLYFOMA without NIR dye and in the presence of IR-813 upon NIR irradiation at 785 nm are presented in Figure 5. The applied irradiance clearly plays a decisive role on the photothermal effect generated. Indeed, the polymer containing IR-813 struggles to reach 60°C after 3 min of irradiation with an irradiance of 0.4 $W.cm^{-2}$ whereas it almost reaches 200°C with an irradiance of 2 $W.cm^{-2}$ (Figure 5B). A very clear linear correlation between the temperature generated in the polymer and the light irradiance can be established with a coefficient of determination $r^2 > 0.97$ (Figure S23, Supporting Information). This correlation is crucial because it allows a predictive and controlled character during the future implementation of materials in 4D printing. In addition, the NIR dye is essential for reaching high temperatures.

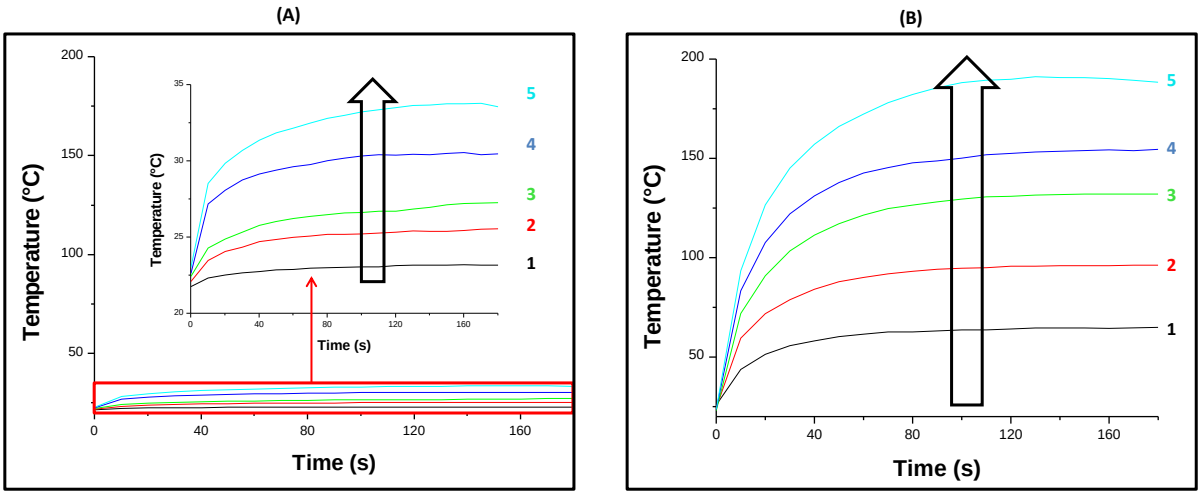

Figure 5. Temperature depending on the irradiation time at 785 nm for polyGLYFOMA (A) without NIR dye ; (B) with 0.1%$_{wt}$ of IR-813 upon an irradiance of (1) 0.4 $W.cm^{-2}$, (2) 0.8 $W.cm^{-2}$, (3) 1.2 $W.cm^{-2}$, (4) 1.6 $W.cm^{-2}$, (5) 2 $W.cm^{-2}$.

By plotting the linear regression lines of the temperatures reached by the polymer depending on the light irradiance at each wavelength for all dyes, it is possible to know the wavelengths in which the NIR dye generates the most effective photothermal effect (Figure S24-30, Supporting Information). Indeed, the better the slope of the linear regression line is,

the most effective the wavelength is. In the same way, it is possible to know the most effective dye at each wavelength (Figure S31-34).

Table 2 groups all the slopes of the linear regression lines established between the temperatures reached by polyGLYFOMA and the irradiances of the light source with highest slopes at each wavelength in red. This table makes possible to know the rise in temperature that the polymer can undergo upon NIR light irradiation, depending on the irradiance of the light source. Thus, the temperature of the reference polymer sample without NIR dye rises by 6.7 ± 0.3°C when the latter is irradiated at 785 nm upon an irradiance of 1 $W.cm^{-2}$. For a polymer sample containing 1%$_{wt}$ of IR-813, it would be 76.3 ± 2.7°C.

These values also confirm the visual impression left by Figure S24-34. Notably, the table shows that the best photothermal effect is reached during the irradiation at 1064 nm in the presence of IR-940. These different slopes are also very interesting as it allows to determine the best combinations of NIR dye, irradiation wavelength and irradiance to be used in order to get a desired temperature when modifying the polymer upon NIR stimulus for 4D printing.

Table 2. Slopes of the linear regression lines for polyGLYFOMA depending on the NIR dye and the irradiation wavelength used.

Colorant	785 nm	940 nm	980 nm	1064 nm
/	6.7 ± 0.3	7.6 ± 0.9	3.0 ± 0.3	6.9 ± 0.5
IR-785	58.1 ± 1.4	24.9 ± 1.1	20.1 ± 1.0	24.6 ± 1.1
IR-813	**76.3 ± 2.7**	26.6 ± 1.8	11.0 ± 0.7	11.8 ± 0.3
IR-850	53.4 ± 1.7	64.6 ± 3.0	69.2 ± 3.7	70.7 ± 3.3
SQ	39.2 ± 3.0	42.2 ± 2.3	42.7 ± 1.3	41.4 ± 2.6
IR-940	48.9 ± 0.7	**72.2 ± 3.0**	**88.9 ± 6.4**	**100.2 ± 1.7**
IR-1064	48.1 ± 2.6	56.4 ± 2.7	61.1 ± 4.0	69.3 ± 1.8

Finally, influence of the monomer used on the photothermal effect generated has been studied. Thus, six different monomers have been used (GLYFOMA, IBOA, TMCHMA, IBOMA, MMA and TMPTA). In order to quantify the influence of the monomer used on the photothermal effect generated in the associated polymer, polymers based on these monomers have been irradiated at 1 $W.cm^{-2}$ upon 5 different wavelengths (785 nm, 850nm, 940 nm, 980 nm and 1064 nm). As shown in Figure S35, Supporting Information, the polymer used has no significant influence on the photothermal effect generated. However, we have previously shown that the NIR dye absorption is strongly influenced by the solvent in which it is introduced. Therefore, the photothermal effect generated will be influenced by the polymer structure in which the NIR dyes will be incorporated.

Thus, polymers in the presence of IR-813 ($0.1\%_{wt}$) were irradiated under the same conditions as reference polymers without NIR dye (Figure S36, Supporting Information). In that respect, polyTMPTA, polyGLYFOMA and polyIBOA generate a better photothermal effect at 785 nm whereas polyMMA is the most effective at 850 nm. Furthermore, polyIBOA is the best polymer at 940 and 980 nm. Finally, there is no significant difference between polymers at 1064 nm according to the very low absorption of IR-813 at this wavelength. In conclusion, it is important to analyze the photothermal effect generated in the polymer used for practical applications if a specific temperature is desired.

3.2. 4D printing using NIR light

In order to know the temperatures which can be reached by the polymer based on a mix between TMPFA and IBOA upon NIR irradiation, 3D printed objects in the absence and in the presence of IR-813 were irradiated 3 min at 810 nm (9 $W.cm^{-2}$) during which the temperature was followed by thermal imaging camera (Figure S37, Supporting Information). The temperature reached by the 3D printed objects without NIR dye is far below that of the 3D printed objects with IR-813 according to the statement provided in the previous part.

Then, the shaping of 3D printed objects was investigated to reach a 4D effect. For this purpose, a simple experiment has been designed and presented on Scheme 3. This experiment consists in placing the 3D printed object on a support and launching the NIR irradiation at 810 nm (9 $W.cm^{-2}$). In the presence of NIR dye, the polymer temperature should increase significantly beyond its T_g, allowing the polymer to achieve new mechanical properties

including polymer deformation. On the other hand, the temperature reached by the reference polymer without NIR dye should be much lower, thus preventing it from accessing the same properties in the same amount of time. The T_g of the 3D printed objects (T_g = 34 °C) has been determined through DSC experiments (Figure S38, Supporting Information).

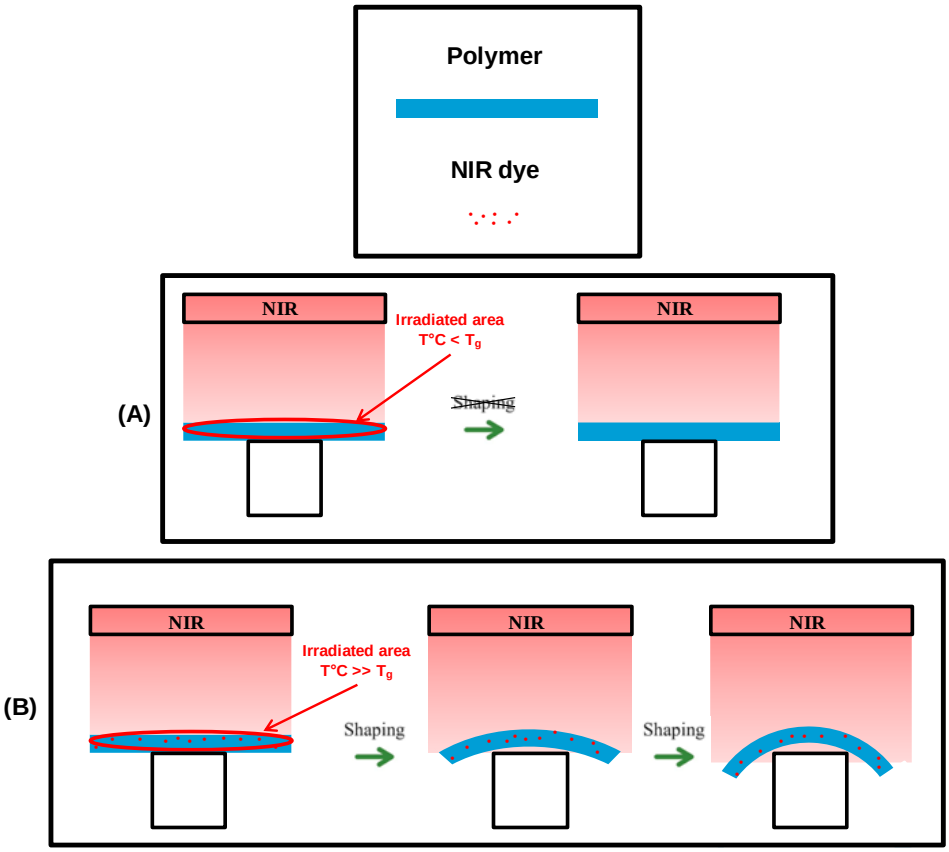

Scheme 3. Polymer behaviour (A) without and (B) with NIR dye upon NIR light source.

The results obtained presented in Figure 6 confirm this rapid deformation of the 3D printed objects when the NIR dye is in-situ embedded in only a few seconds (20s). On the other hand, the temperature reached by the reference 3D printed object without NIR dye is not as high under NIR irradiation (37°C vs 78°C), preventing it from accessing the same properties in the same amount of time. Furthermore, the maximal temperature reached by the reference polymer is concentrated on the part in direct contact with the support whereas the rest of the polymers keeps a much lower temperature. Consequently, the maximal temperature reached by the 3D printed object is in this case mainly due to an energy transfer between the base and the polymer, not to the direct irradiation of the light source.

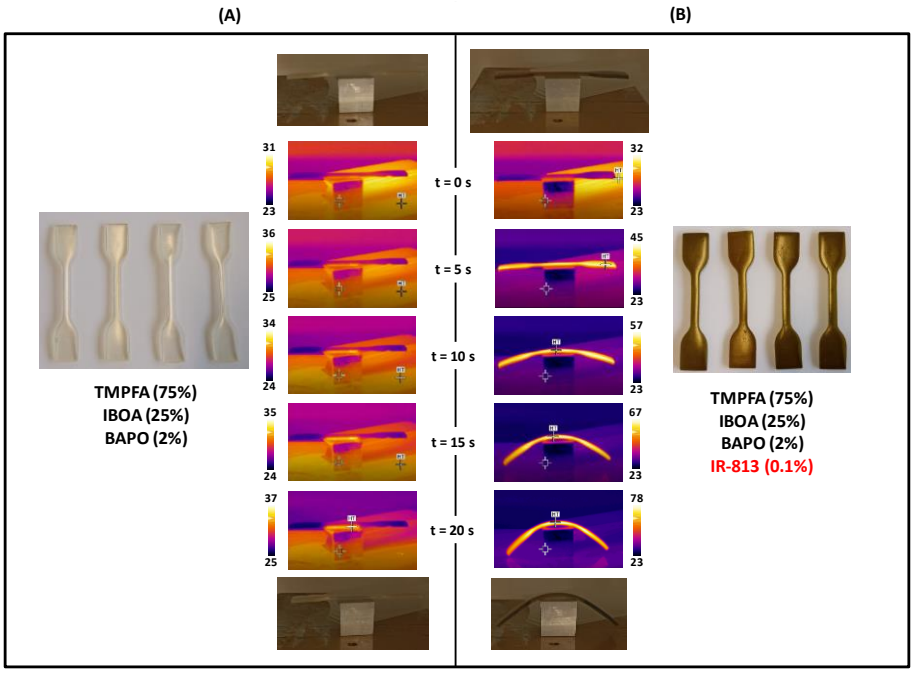

Figure 6. Modification of the 3D printed polymer shape by irradiation upon a NIR LED panel at 810 nm (9 W.cm^{-2}).

Thereafter, the possibility of carrying out deformation cycles has been tested. To that end, an experiment was set up. Scheme 4A describes the cycle which can be separated in two steps. The first step consists in shaping the polymer as previously shown in Scheme 3. In the second step, the reversibility of this shaping can be examined by submitting the 3D printed object once more to NIR light to end the cycle (Scheme 4B).

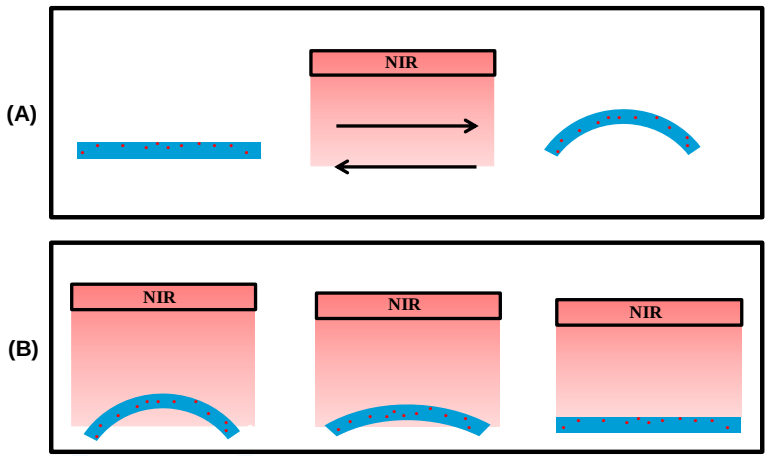

Scheme 4. (A) Shaping cycle of a 3D printed polymer in the presence of NIR dye. (B) 3D printed polymer shape modification to make it back to its initial shape.

Thus, the shaped 3D printed object was placed under the LED panel at 810 nm (9 $W.cm^{-2}$) and monitored by thermal imaging camera as shown in Figure 7. This figure confirms the reversibility of the shaping. It is indeed possible to return back to the original shape very quickly, in less than only 20 s.

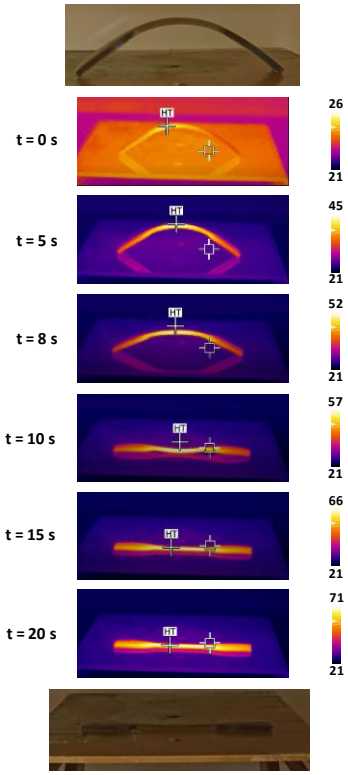

Figure 7. Modification of the 3D printed polymer shape by irradiation upon a NIR LED panel at 810 nm (9 $W.cm^{-2}$) to make it return to its original shape.

Then, tensile tests were performed at 22°C on the 3D printed objects containing IR-813 to get information about their behavior under stress (Figure 8). In that respect, tensile tests without NIR light were performed on 3D printed samples and compared with tensile tests performed after 3 min of NIR irradiation, the latter being maintained during the tensile test. After irradiating the 3D printed objects for 3 min., the tensile curves are completely different than before irradiation. Indeed, tensile curves obtained before NIR irradiation are characteristic of thermoplastic polymers when they are below their T_g. In fact, the curves are marked by a flow threshold which corresponds to the necking phenomenon. On the opposite, tensile curves obtained after 3 min of NIR irradiation are characteristic of thermoplastic polymers when their temperatures are beyond their T_g.[31]

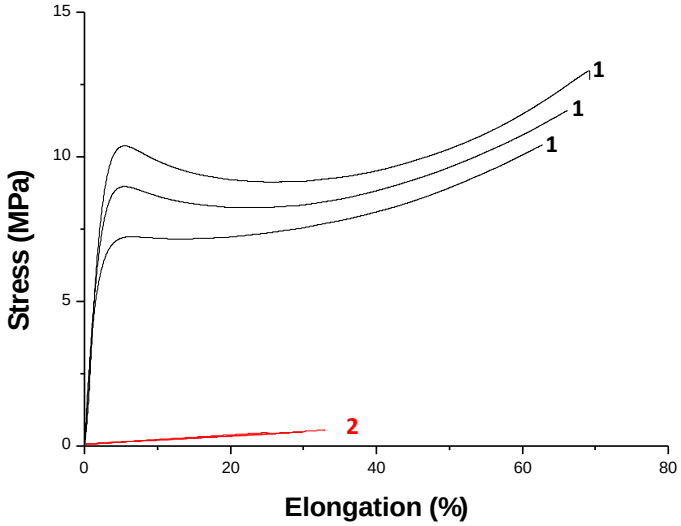

Figure 8. Tensile tests with a speed spacing of 10 mm.min^{-1} and an initial spacing between jaws of 40 mm for 3D printed polymers containing 0.1%$_{wt}$ of IR-813 (1) without NIR irradiation and (2) after 3 min of NIR irradiation. T_i = 22°C.

Young modulus, rupture strengths and elongations of tensile tests were also investigated and the results are presented in Table 3. Huge differences can be noted between irradiated and non-irradiated 3D printed samples. Notably, the Young modulus and the rupture strength are respectively 300 and 20 times greater before NIR irradiation. In fact, the temperature in the 3D printed object is so high upon NIR light source (~200°C) that it becomes very malleable.

Table 3. Determination of Young modulus, rupture strength and maximal elongation of 3D printed polymers (1) without NIR dye and before NIR irradiation, (2) without NIR dye and after 3 min of NIR irradiation, (3) with IR-813 and before NIR irradiation, (4) with IR-813 and after 3 min of NIR irradiation.

Colorant	Young modulus (MPa)	Rupture strength (MPa)	Elongation (%)
1	435.4 ± 43.3	11.7 ± 1.3	66.0 ± 3.2
2	1.5 ± 0.1	0.5 ± 0.0	28.9 ± 3.9

Finally, a simple experiment has been designed to bond two parts of a broken 3D printed sample as shown in Figure 9. The two parts were put in contact and irradiated 2 min upon NIR light at 785 nm (2 $W.cm^{-2}$). The temperature reached by the parts in contact is high enough to go above the T_g of the 3D printed samples (34°C). After cooling the sample below the T_g of the samples, the bonding was completed. The bonded 3D printed polymer can afterwards be debonded by re-irradiating the sample upon NIR light.

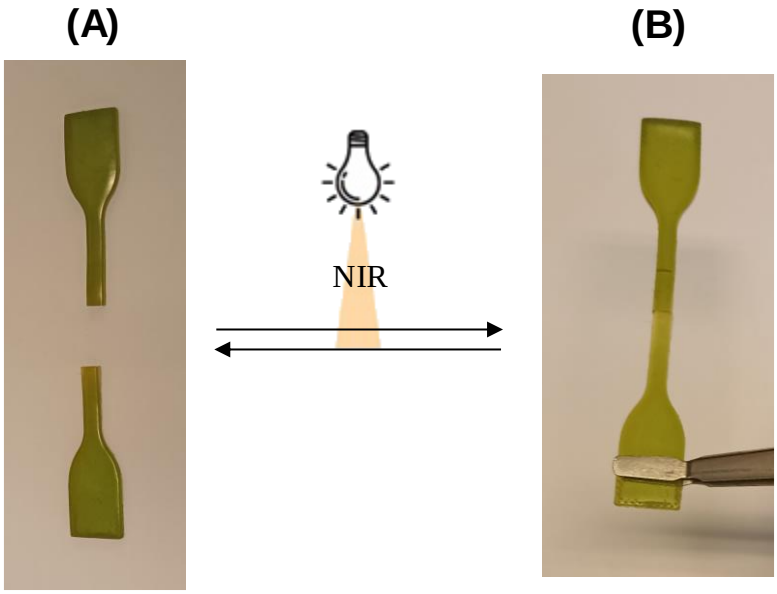

Figure 9. Photos of bonding/debonding experiments (A) before and (B) after NIR irradiation of two 3D printed objects containing 0.1%$_{wt}$ of IR-813. Irradiation performed 2 min at 785 nm (2 $W.cm^{-2}$).

4. Conclusion

In conclusion, the photothermal effect in-situ generated in polymers using NIR organic dyes has been studied. Notably, the influence of several factors such as the NIR dye structure, the NIR dye concentration, the irradiation wavelength, the light irradiance and the polymer matrix have been deeply investigated. In addition, the shape modification of 3D printed objects was studied. The importance of using a low concentration ($0.1\%_{wt}$) of the NIR dye in-situ embedded in the 3D printed object allowed a rapid rise in temperature of the polymer upon NIR light resulting in a rapid modification (a few seconds) of the 3D printed object shape. The reversibility of the phenomenon has also been demonstrated. The mechanical properties of the 3D printed object were also investigated through tensile tests. The latter notably showed the passage of the 3D printed object from a glassy state to a rubbery state upon NIR irradiation, the Young modulus falling from 435 MPa before NIR irradiation to 2 MPa after 3 min of NIR irradiation. Finally, the bonding of broken 3D printed objects was successfully performed. These different experiments allowed the 3D printed object to achieve 4D properties.

References

[1] Hahladakis, J.N., Iacovidou, E. *Closing the loop on plastic packaging materials: What is quality and how does it affect their circularity?* Science of The Total Environment 2018, 630, 1394–1400.

[2] Dutta, S., Nadaf, M.B., Mandal, J.N. *An Overview on the Use of Waste Plastic Bottles and Fly Ash in Civil Engineering Applications*. Procedia Environmental Sciences 2016, 35, 681–691.

[3] Aurisano, N., Huang, L., Milà i Canals, L., Jolliet, O., Fantke, P. *Chemicals of concern in plastic toys*. Environment International 2021, 146, 106194.

[4] Liaw, C.-Y., Guvendiren, M. *Current and emerging applications of 3D printing in medicine.* Biofabrication 2017, 9(2), 024102.

[5] Espera, A.H., Dizon, J.R.C., Chen, Q., Advincula, R.C. *3D-printing and advanced manufacturing for electronics.* Progress in Additive Manufacturing 2019, 4(3), 245-267.

[6] Vanderploeg, A., Lee, S.-E., Mamp, M. *The application of 3D printing technology in the fashion industry. International Journal of Fashion Design.* Technology and Education 2016, 10(2), 170–179.

[7] Tay, Y.W.D., Panda, B., Paul, S.C., Noor Mohamed, N.A., Tan, M.J., Leong, K.F. *3D printing trends in building and construction industry: a review.* Virtual and Physical Prototyping 2017, 12(3), 261–276.

[8] Uriondo, A., Esperon-Miguez, M., Perinpanayagam, S. *The present and future of additive manufacturing in the aerospace sector: A review of important aspects.* Proceedings of the Institution of Mechanical Engineers, Part G: Journal of Aerospace Engineering 2015, 229(11), 2132–2147.

[9] Ma, X.L. *Research on Application of SLA Technology in the 3D Printing Technology.* Applied Mechanics and Materials 2013, 401-403, 938–941.

[10] Kadry, H., Wadnap, S., Xu, C., Ahsan, F. *Digital light processing (DLP) 3D-printing technology and photoreactive polymers in fabrication of modified-release tablets.* European Journal of Pharmaceutical Sciences 2019, 135, 60–67.

[11] Shan, J., Yang, Z., Chen, G., Hu, Y., Luo, Y., Dong, X., Zheng, W., Zhou, W. *Design and Synthesis of Free-Radical/Cationic Photosensitive Resin Applied for 3D Printer with Liquid Crystal Display (LCD) Irradiation. Polymers 2020, 12(6), 1346.*

[12] Moller, J.C., Berry, R.J., Foster, H.A. *On the Nature of Epoxy Resin Post-Curing.* Polymers 2020, 12(2), 466-485.

[13] Salmoria G.V., Gonzalez V.J., Ahrens C.H., Soldi V., Pires A.T.N. *StereolithographySomos 7110 photosensitive resin: study of curing kinetic and thermaldegradation*. Journal of Materials Processing Technology 2005, 168(11), 164–171.

[14] Salmoria G.V., Ahrens C.H., Fredel M., Soldi V., Pires A.T.N. *Stereolithography Somos7110 resin: mechanical behaviour and fractography of parts post-cured bydifferent methods*. Polymer Testing 2005, 24(2), 157–162.

[15] Reymus M., Lümkemann N., Stawarczyk B. *3D-printed material for temporary restorations: impact of print layer thickness and post-curing method on degree of conversion*. International Journal of Computerized Dentistry 2019, 22(3), 231-237.

[16] Reymus, M., Fabritius, R., Keßler, A., Hickel, R., Edelhoff, D., Stawarczyk, B. *Fracture load of 3D-printed fixed dental prostheses compared with milled and conventionally fabricated ones: the impact of resin material, build direction, post-curing, and artificial aging—an in vitro study.* Clinical Oral Investigations 2019, 24(2), 701-710.

[17] Bonada, J., Muguruza, A., Fernández-Francos, X., Ramis, X. *Influence of exposure time on mechanical properties and photocuring conversion ratios for photosensitive materials used in Additive Manufacturing.* Procedia Manufacturing 2017, 13, 762–769.

[18] Tibbits, S. The emergence of « 4D printing », https://www.youtube.com/watch?v=0gMCZFHv9v8 (visited on the 23rd of March 2022).

[19] Su, J.-W., Tao, X., Deng, H., Zhang, C., Jiang, S., Lin, Y., Lin, J. *4D printing of a self-morphing polymer driven by a swellable guest medium.* Soft Matter 2018, 14(5), 765–772.

[20] Hu, Y., Wang, Z., Jin, D., Zhang, C., Sun, R., Li, Z., Hu, K., Ni, J., Cai, Z., Pan, D., Wang, X., Zhu, W., Li, J., Wu, D., Zhang, L., Chu, J. *Botanical-Inspired 4D Printing of Hydrogel at the Microscale.* Advanced Functional Materials 2019, 30(4), 1907377.

[21] Mao, Y., Yu, K., Isakov, M. S., Wu, J., Dunn, M. L., Jerry Qi, H. *Sequential Self-Folding Structures by 3D Printed Digital Shape Memory Polymers.* Scientific Reports 2015, 5(1), 13616.

[22] Kim, Y., Yuk, H., Zhao, R., Chester, S. A., Zhao, X. *Printing ferromagnetic domains for untethered fast-transforming soft materials.* Nature 2018, 558(7709), 274–279.

[23] Garcia Rosales, C., Garcia Duarte, M., Kim, H., Chavez, L., Hodges, D., Mandal, P., Lin, Y., Tseng, T.-L. *3D printing of shape memory polymer (DMP)/carbon black (CB) nanocomposites with electro-responsive toughness enhancement.* Materials Research Express 2018, 5(6), 065704.

[24] Ryu, J., D'Amato, M., Cui, X., Long, K.N., Jerry Qi, H., Dunn, M. L. *Photo-origami—Bending and folding polymers with light.* Applied Physics Letters 2012, 100(16), 161908.

[25] Launay, V., Caron, A., Noirbent, G., Gigmes, D., Dumur, F., Lalevée, J. *NIR organic dyes as innovative tools for reprocessing/recycling of plastics: Benefits of the photothermal activation in the near-infrared range*. Advanced Functional Materials 2020, 31(7), 2006324.

[26] Launay, V., Dumur, F., Gigmes, D., Lalevée, J. *Near-infrared light for polymer re-shaping and re-processing applications*. Journal of Polymer Science 2021, 59(19), 2193-2000.

[27] Launay, V., Pieuchot, L., Dumur, F., Lalevée, J. *Safe Near Infrared Light for Fast Polymers Surface Sterilization using Organic Heaters*. Materials Chemistry Frontiers 2022, DOI: 10.1039/D1QM01609A.

[28] Strassel, K., Kaiser, A., Jenatsch, S., Véron, A.C., Anantharaman, S.B., Hack, E., Diethelm, M., Nüesch, F., Aderne, R., Legnani, C., Yakunin, S., Cremona, M., Hany, R. *Squaraine Dye for a Visibly Transparent All-Organic Optical Upconversion Device with Sensivity at 1000 nm*. ACS Applied Materials & Interfaces 2018, 10(13), 11063-11069.

[29] Yan, X., Zhao, L., Liu, Y., Xing, R. *Supramolecular photothermal effects: A promising mechanism for efficient thermal conversion.* Angewandte Chemie International Edition 2020, 59(10), 3793-3801.

[30] Law, K-Y. *Squaraine Chemistry: Effects of Structural Changes on the Absorption and Multiple Fluorescence Emission of Bis[4-(dimethylamino)phenyl]squaraine and Its Derivatives*. The Journal of Physical Chemistry 1987, 91(20), 5184-5193.

[31] Kitagawa, M., Zhou, D., Qui, J. *Stress-Strain curves for solid polymers.* Polymer Engineering and Science 1995, 35(22), 1725–1732.

TOC graphic :

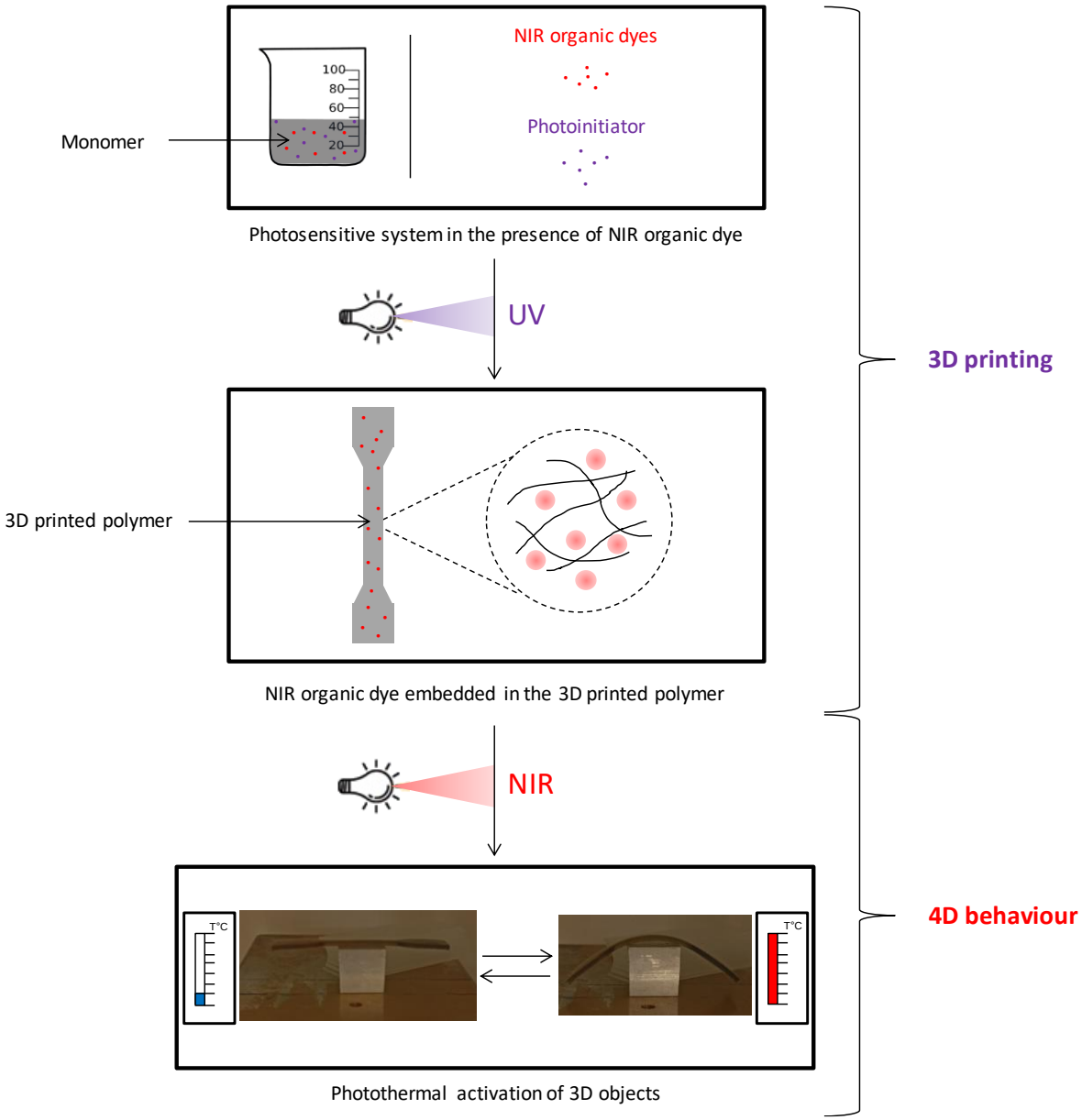
NIR organic dyes
Photoinitiator
Monomer
100
80
60
40
20
Photosensitive system in the presence of NIR organic dye
UV
3D printing
3D printed polymer
NIR organic dye embedded in the 3D printed polymer
NIR
4D behaviour
T°C
T°C
Photothermal activation of 3D objects